Systematic design of broadband path-coiling acoustic metamaterials

Zhetao Jia, Junfei Li, Chen Shen, Yangbo Xie, and Steven A. Cummer[a)]
Department of Electrical and Computer Engineering, Duke University, Durham, North Carolina 27708, USA

(Received 17 October 2017; accepted 21 December 2017; published online 8 January 2018)

A design approach for acoustic metamaterial unit cells based on a coiled path with impedance matching layers (IMLs) is proposed in this paper. A theoretical approach is developed to calculate the transmission of the labyrinthine unit cells with different effective refractive indices. The IML is introduced to broaden the transmission bandwidth and produce a lower envelope boundary of transmission for unit cells of different effective refractive indices. According to the theory, cells of all effective refractive indices can be built to achieve unitary transmission at center working frequencies. The working frequency can be tuned by adjusting the length of the IML. Numerical simulations based on finite element analysis are used to validate the theoretical predictions. The high transmission and low dispersive index nature of our designs are further verified by experiments within a broad frequency band of over 1.4 kHz centered at 2.86 kHz. Our design approach can be useful in various wavefront engineering applications. *Published by AIP Publishing.*
https://doi.org/10.1063/1.5009488

I. INTRODUCTION

Acoustic metamaterials, with their flexible and even exotic proprieties such as negative density and negative bulk modulus, provide new possibilities in controlling acoustic propagation and wave fields.[1–3] By building up the structure using subwavelength units of different properties, extraordinary manipulation of sound propagation can be achieved. Acoustic metasurfaces, as a sub-category of acoustic metamaterials, have attracted much research effort in recent years due to their thin structure and outstanding ability in wavefront engineering.[2,4–8] The increasing interest in acoustic metasurface calls for the search of high transmission metamaterial unit cells with strong local phase control capability. In most scenarios, the performance of the metasurface is determined by the property of the individual unit cell, of which many designs have been proposed in the past few years.[5,9–11] The idea of path-coiling, where the incident acoustic wave is guided into narrow zig-zag channels coiled up in space, was first proposed by Liang and Li[12] in order to produce high index and negative refraction unit cells. The acoustic path-coiling metamaterial was then proven to support high transmission close to the Fabry-Pérot resonant frequency with subwavelength cell size.[13] By choosing suitable channel width and path length, the unit cell can cover a complete 2π phase change across the structure. The design strategy has been used in various applications of wavefront engineering, such as beam-bending, acoustic focusing, hologram imaging, etc.[5–7,11,14,15]

However, such resonance-based acoustic metamaterial unit cells suffer from a narrow bandwidth, as high transmission only exists near the resonant frequencies. When the frequency of the incident wave is off resonance, the impedance mismatch between the narrow channel and the surrounding background medium at the entrance leads to high reflection. In order to circumvent this problem, impedance matching layers (IMLs) have been introduced in a helical cell design to allow better impedance matching.[16,17] However, no analytical solution has been formulated to predict the property of the transmitted wave with an IML present, and the proposed helical designs are unable to tessellate the metasurface which causes part of incident energy to get reflected, scattered or absorbed by the metamaterial structure in real applications. In addition, to ensure precise phase control over the 2π range, the path length has to be changed for different unit cells. However, one drawback of this process is that it shifts the resonant frequency and it is therefore hard to find a common working frequency range for a set of metamaterial unit cells of different effective refractive indices to guarantee high transmission. Previous work aimed at solving this problem is based on optimization and more than one parameter is required to be adjusted to design cells of different indices.[4,5,10,11,16] Another drawback is that instead of the indices, only the output phase is considered in these designs which sacrifices the possibility for the cells to be applied in broadband applications. So far, a simple and systematic way to generate a set of broadband unit cells with unit transmission at a common working frequency remains an open problem.

In this paper, we develop a design approach for a set of labyrinthine metamaterial unit cells of different indices with shared, controllable working frequency and bandwidth. An analytic model is developed to theoretically calculate the transmission of unit cells. It is also found that by adding IMLs, there exists a lower boundary of transmission of a set of cells with different indices. Due to the lowest transmission envelope which predicts the lower bound of the transmission coefficient, high transmission of all the unit cells in a certain frequency range is guaranteed. The IMLs also broaden the bandwidth of the transmission peak. Our design approach is further verified in both simulation and experiment. The design scheme can be easily modified to satisfy specific requirements for different applications which need

[a)]Author to whom correspondence should be addressed: cummer@ee.duke.edu

metamaterial unit cells of different indices in a wide frequency range.

II. THEORY

First consider a rectangular channel with open ends, when the frequency of the propagating mechanical wave is lower than the cut-off frequency of the waveguide, no high order mode is supported. The acoustic field inside the channel can be treated as a plane wave; hence, resonant frequencies are

$$f = n\frac{c}{2L}(n = 1, 2, 3\ldots), \tag{1}$$

where c is the speed of sound and L is the length of the channel. The zig-zag path can be added to the straight channel to slow the acoustic wave propagating from one end to the other. This slow-sound effect is characterized by the refractive index of the medium, which is defined as the ratio of sound speed in the medium compared with that in air for the homogeneous material. The path-coiled channel can be equivalent to an effective homogeneous medium connecting two ends of the waveguide directly. For a single mode waveguide with a normal incident plane wave, the sound transmits slower because of the coiled path length. Hence, the effective refractive index can be estimated by $n_{eff} = \frac{L_{eff}}{L_0}$, where L_{eff} is the zig-zag effective path length of the acoustic wave propagation and L_0 is the distance between two ends of the channel along the wave propagation direction.[11] When the effective path length is changed to build cells of different effective refractive indices, the shift of the resonant frequency according to Eq. (1) would prevent cells of different refractive indices to share a common resonant frequency. It is therefore difficult to ensure high transmission for different unit cells at a certain frequency and this drawback severely hinders their applications in real-world problems. To solve this problem, we proposed a new design strategy for a set of labyrinthine acoustic metamaterial unit cells and an example is shown in Fig. 1(a). The top view of the design is shown in Fig. 1(b), where the acoustic wave is guided into a narrower channel of width S_4 through an IML of width S_2.

To calculate the overall transmission of the labyrinthine unit cell design, we first unpack the coiled path into a connecting tube structure shown in Fig. 1(d), where segments with the same channel width have the same effective path length. It will be shown that this configuration can be used to estimate the far-field transmission of the labyrinthine metamaterial unit cell with the zig-zag path shown in Fig. 1(b). Both ends of the structure (channels of width S_1) are assumed to be infinitely long and the channels of width S_2, S_4, and S_6 extend the length L_2, L_4, and L_6, respectively. The width of the structure is smaller than half of the acoustic wavelength, so only plane waves are allowed. At each tube intersection, the continuity of pressure and the volume velocity reads

$$p_n = p_{n+1}, \tag{2a}$$

$$U_n = U_{n+1}\ (n = 1,\ 3,\ 5,\ 7), \tag{2b}$$

where p_n and U_n are the pressure and the volume velocity close to the channel intersection labeled with n in Fig. 1(d), respectively. Because the specific acoustic impedance z_n, by definition, is related to the volume velocity by $z_n = \frac{p_n}{u_n} = \frac{p_n}{U_n}S_n$, where u_n represents the velocity and S_n is the channel width

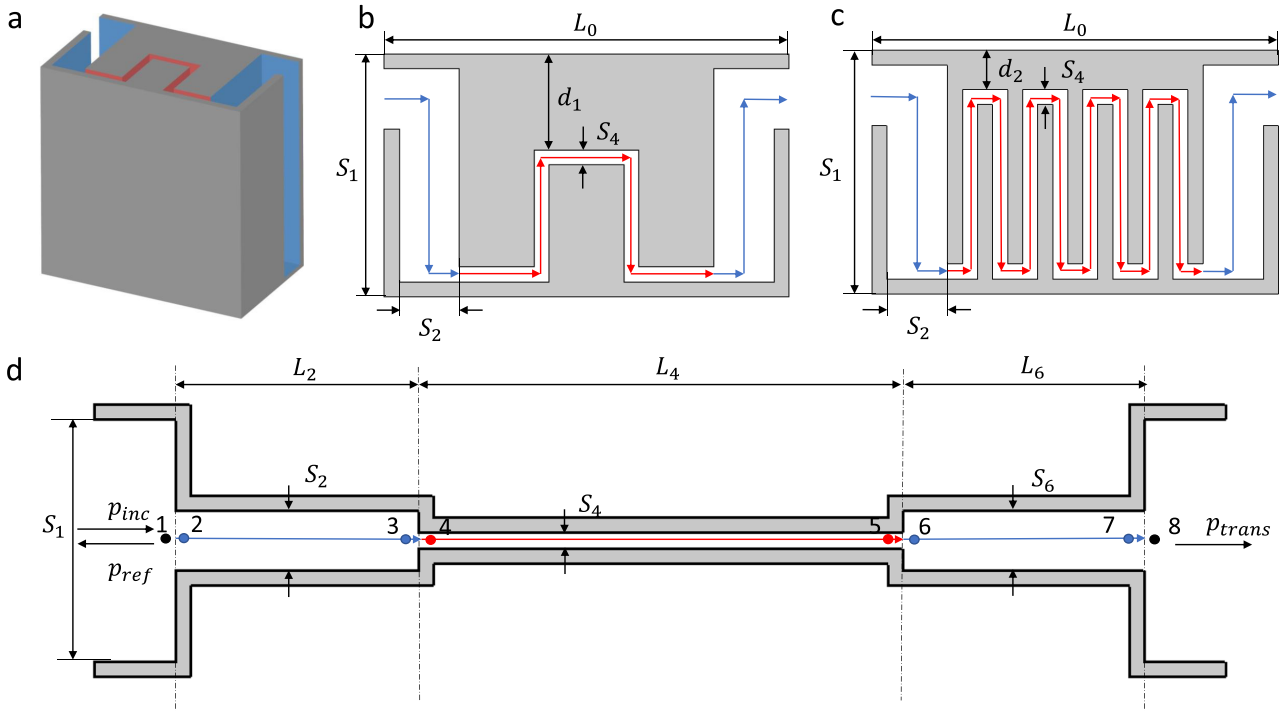

FIG. 1. Acoustic metamaterial unit cells and the unpacked connecting tube structure. (a) An example of 3D model of the unit cell is shown. Different colors represent channels of different widths. (b) Top view of the unit cell shown in (a) where the arrowed lines indicate the effective path of the incident acoustic wave. (c) An acoustic metamaterial unit cell with a higher effective refractive index is formed by increasing the length of the narrowest channel. (d) The equivalent connecting tube structure is obtained by expanding the coiled path with the same effective path length at each channel width for the labyrinthine unit cell shown in (b).

near the intersection labeled n. The channel width is proportional to the area of cross section as each channel shares the same height. Equation (2b) can be replaced by

$$\frac{z_n}{S_n} = \frac{z_{n+1}}{S_{n+1}}. \tag{2c}$$

Since the channel widths are much smaller than the operation wavelength, only planes waves exist inside the channels. The pressure and velocity field can thus be represented as

$$\begin{aligned} p(x,t) &= P_+ e^{j(\omega t - kx)} + P_- e^{j(\omega t + kx)} \\ u(x,t) &= \frac{1}{\rho c}\left(P_+ e^{j(\omega t - kx)} - P_- e^{j(\omega t + kx)}\right), \end{aligned} \tag{3}$$

where ω is the angular frequency of the plane wave and $k = \frac{2\pi}{\lambda}$ is the wavenumber. P_+ and P_- represent the coefficient of forward and backward travelling waves, respectively. Along the channel of the same width, the pressure and acoustic impedance at two ends can be related by the following equation according to Eq. (3):[18]

$$\begin{aligned} p_{n+1} &= \frac{p_n}{z_n}(z_n \cos kL_n - i\rho c \sin kL_n) \\ z_n &= \rho c \frac{z_{n+1}\cos kL_n + i\rho c \sin kL_n}{\rho c \cos kL_n + i\, z_{n+1} \sin kL_n} \ (n = 2,\ 4,\ 6), \end{aligned} \tag{4}$$

where ρ is the density of the medium and c is the acoustic wave propagation speed. At the entrance [label 1 in Fig. 1(d)], the pressure and the acoustic impedance can be represented by

$$\begin{aligned} p_1 &= p_{inc} + p_{ref} \\ z_1 &= \frac{p_1}{u_1} = \frac{\rho c(p_{inc} + p_{ref})}{p_{inc} - p_{ref}}. \end{aligned} \tag{5}$$

Hence, the pressure of the incident wave can be related to the pressure close to label 1 by

$$p_1 = \frac{2p_{inc}}{1 + \frac{\rho c}{z_1}}. \tag{6}$$

At the exit of the tube, there is no left-propagating wave as the end of the tube has anechoic termination

$$p_8 = p_{trans}. \tag{7}$$

The connecting channel structure is designed to be symmetric, where $L_2 = L_6$ and $S_2 = S_6$. The channel width of the intermediate layer is chosen to be $S_2 = \sqrt{S_1 S_4}$ to meet the impedance matching condition for the specific impedance $z_2 = \sqrt{z_1 z_4}$.[19] Combining Eqs. (2), (4), (6), and (7), the overall complex transmission can be obtained using Mathematica as

$$\begin{aligned} T &= \frac{p_t}{p_i} = \frac{2S_1 S_4}{\sqrt{M^2 + N^2}} \\ M &= \sqrt{S_1 S_4}(S_1 + S_4)\cos kL_4 \sin 2kL_2 \\ &\quad + \left(S_1^2 + S_4^2\right)\cos^2 kL_2 \sin kL_4 - 2S_1 S_4 \sin^2 kL_2 \sin kL_4 \\ N &= -2S_1 S_4 \cos^2 kL_2 \cos kL_4 + 2S_1 S_4 \cos kL_4 \sin^2 kL_2 \\ &\quad + \sqrt{S_1 S_4}(S_1 + S_4)\sin 2kL_2 \sin kL_4. \end{aligned} \tag{8}$$

A similar derivation can be found in Jones and Kessissoglou[20] The transmission amplitude and phase shift at the output can be calculated by taking the absolute value and the argument of T, respectively. The transmission amplitude $T_{amp} = Abs(T)$ is a function of the narrowest channel length L_4. By setting the derivative of the absolute value of T_{amp} to zero $\frac{\partial T_{amp}}{\partial L_4} = 0$, the lowest transmission amplitude for the connecting tube structure with any length of the narrowest channel L_4 is reached at

$$\cos kL_4 = \frac{2\sqrt{2S_1 S_4}\sin kL_2}{\sqrt{S_1^2 + 6S_1 S_4 + S_4^2 + (S_1 - S_4)^2 \cos 2kL_2}}. \tag{9}$$

Inserting the condition Eq. (9) back to the expression of transmission Eq. (8) and taking the absolute value for amplitude, the lower boundary of the transmission for different L_4 can be written as

$$T_{min} = \frac{4\eta}{(1+\eta)^2 + (1-\eta)^2 \cos 2kL_2}, \tag{10}$$

where $\eta = \frac{S_4}{S_1}$ is the ratio of the channel width and wavenumber $k = \frac{2\pi f}{c}$. From Eq. (10), we can see that the lower boundary of transmission at certain frequency f depends only on the ratio of the channel width η and the length of the IML (L_2) along the wave propagation direction in the homogenous medium. The center frequencies of the envelope line can be found at $f = \frac{(2n+1)c}{4L_2}$ $(n = 0,\ 1,\ 2\ldots)$ with the first resonance peak at $f_0 = \frac{c}{4L_2}$. At these resonant frequencies, the transmission achieves unity, which is independent of the path length of the narrowest channel L_4. It is worth noticing that at the first order resonant frequency, the IMLs function as quarter-wave plates to allow all the incident energy to get transmitted. Unit cells of any effective path length can thus be built conveniently with unitary transmission at those working frequencies without changing other parameters in the design. The bandwidth can be determined by solving the full width at half maximum expression, i.e., $T_{min} \geq \frac{1}{2}$. The results show that the bandwidth is also inversely proportional to the IML length L_2 and becomes larger for smaller ratio η as long as the plane wave assumption is valid. By adjusting the length of the IML (L_2) and the ratio of the channel width η, the lower boundary of the transmission of structures with different path lengths can be controlled. Comparing the metamaterial design in Fig. 1(b) and its corresponding expanded structure in Fig. 1(d), we expect the net transmission is unaffected by the unpacking process because the mechanical wave propagates by disturbing the adjacent medium. The correctness of this claim is shown via simulation in Section III.

III. SIMULATION AND EXPERIMENT

To demonstrate the design approach developed in the Section II, we design a set of cells of different indices and compare the connecting tube theory with the simulation result of the labyrinthine unit cells. The length of the unit cell is fixed at $L_0 = 50.0\,\text{mm}$. According to Eq. (10), the

bandwidth is broader for the higher channel width ratio and the narrowest channel width is chosen to be $S_1 = 30\,\text{mm}$ and $S_4 = 1.85\,\text{mm}$ with the ratio of channel width $\eta = 0.062$ for fabrication consideration. The width of the IML normal to the wave propagation direction is determined by $S_2 = \sqrt{S_1 S_4} = 7.44\,\text{mm}$. The equivalent length of each IML (L_2) [blue lines in Figs. 1(b) and 1(d)] is 30 mm for a center working frequency $f_0 = \frac{c}{4L_2} = 2.86\,\text{kHz}$, which guarantees the size of the unit cell to be smaller than half of the corresponding wavelength $\lambda = 120\,\text{mm}$. The path-coiling parameters of the two designs shown in Figs. 1(b) and 1(c) are $d_1 = 10\,\text{mm}$ and $d_2 = 3\,\text{mm}$, respectively, corresponding to the equivalent narrowest path length (L_4) 60 mm and 201 mm obtained from the length of effective acoustic paths shown as red lines. The simulation is performed using the Finite Element Method with the COMSOL acoustic module in two dimensions, where a plane wave is sent to illuminate the structure. Figure 2 shows a comparison of the connecting tube theory prediction and COMSOL simulation result for the two cell structures displayed in Figs. 1(b) and 1(c). For both the transmission coefficient and index of the labyrinthine cell, the theoretical prediction agrees well with the simulation, which confirms that the path-coiling process has a negligible influence on the far-field transmission. In simulation, the complex amplitude at the far field is recorded and the phase shift caused by the cell is used to compute the effective refractive index of the cell. In Figs. 2(b) and 2(d), both simulation and theory show the low dispersion of the labyrinthine design where the standard deviation of the index in the simulation of each cell is less than 6.5% of its average value in the range from 2.2 kHz to 3.6 kHz, which is the working frequency range for the designed unit cells with any index as we will show next.

To verify the existence of the envelope line based on the connecting tube theory, simulated transmission of seven labyrinthine unit cells with different narrowest path lengths is shown in Fig. 3(a). The narrowest path lengths (L_4) at regular intervals range from 30 mm to 230 mm, which correspond to the shortest and longest narrowest channel length available for the cell size we choose. The cells are designed to minimize the number of turning points in the acoustic path and the detailed parameters are shown in the supplementary material. Besides, the simulation results of two unit cells shown in Figs. 1(b) and 1(c) with narrowest channel length 60 mm and 201 mm are also included. The lowest transmission of the seven cells at each simulated frequency is marked with a cross, which is well-predicted by Eq. (10) derived from the connecting tube theory as the red line in Fig. 3(a). The envelope line allows continuous index change based on labyrinthine unit cells with different path lengths over a

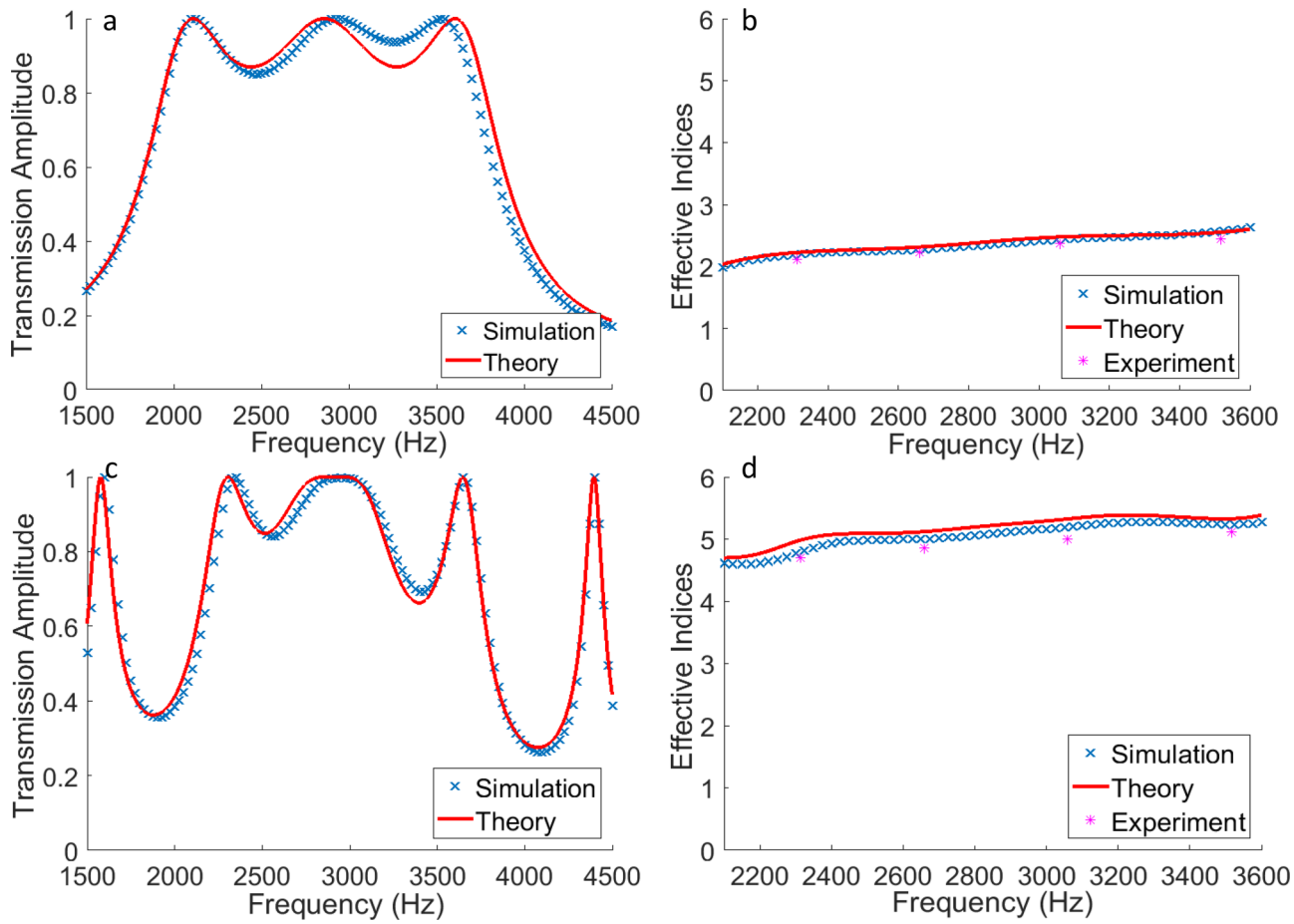

FIG. 2. Simulated (cross mark) and theoretically calculated (red curve) transmission amplitudes and effective refractive indices of the acoustic metamaterial unit cells. (a) and (b) Transmission amplitude and effective refractive indices of lossless simulation and theoretical result for the unit cell shown in Fig. 1(b). (c) and (d) Transmission amplitude and effective refractive indices of lossless simulation and theoretical result for the unit cell shown in Fig. 1(c). The error bars for experiments are not shown as the standard deviation of each value is less than 3%.

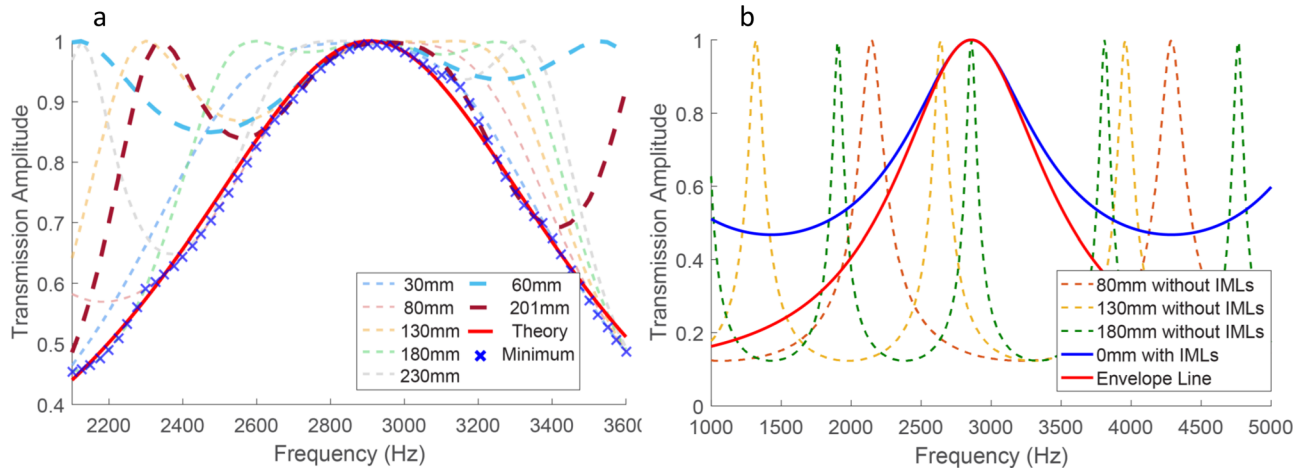

FIG. 3. Comparison of simulated transmission of metamaterial unit cells of narrowest path lengths (L_4) and theoretically predicted envelope line based on the connecting tube structure [Fig. 1(d)]. (a) The dashed lines are the simulated transmission amplitude for unit cells with labeled narrowest channel lengths and the cross marker selects the lowest among seven transmission amplitudes at each sampling frequency. The red line is the theoretically calculated envelope line according to Eq. (10). (b) The red line is the same transmission envelope which is shown in Fig. 3(a). The dashed lines represent the tranmission amplitudes without the IMLs. The blue curve shows the transmission with the IML only and without the narrowest path ($L_4 = 0$).

bandwidth of 1.4 kHz centered at 2.86 kHz, where the transmission amplitude is greater than 0.5.

The improvement of performance in transmission after inserting the IML is shown in Fig. 3(b), where the calculated transmission without the IML is shown as dashed lines. In the case of no IML, the acoustic wave is guided from the channel of width S_1 into another channel of S_4 directly and the result shows a relatively narrow bandwidth as well as a shift of the Fabry-Pérot resonant frequency for cells with effective narrowest path length L_4. This is not surprising as the structure is resonance-based. On the other hand, the bandwidth is dramatically broadened after the IML is introduced, as can be seen in Fig. 3(b). According to the comparison in Fig. 3(b), the IML guarantees a lowest boundary with bandwidth 4–10 times greater than the original design and eliminates the problem of resonant frequency shift which makes coordination of different cells challenging for previous designs. It is also interesting to consider the extreme case for the narrowest path length $L_4 = 0$, where the acoustic wave propagates from the channel of width S_1 through two connected IMLs of width S_2 and back to S_1 for the tube structure similar to Fig. 1(d). Its transmission [blue line in Fig. 3(b)] is above the envelope line as predicted and its resonant frequencies $f_{L_4=0} = m\frac{c}{4L_2}(m = 0, 1, 2\ldots)$ from Eq. (1), while the centers of the envelop line locate at $f_n = (2n+1)\frac{c}{4L_2}$ $(n = 0, 1, 2\ldots)$. The comparison indicates that by inserting a narrower channel of width S_4, arbitrary phase delay can be introduced around the center frequency at a cost of degraded transmission around the original even Fabry-Pérot resonance modes. Based on Eq. (10), the transmission amplitude envelope with respect to different channel width ratios and wavelength-impedance layer length ratios is shown in Fig. 4. For the cells we used in this paper $(\eta = 0.062)$, the corresponding envelope line is displayed in red. According to Fig. 4, the bandwidth can be further broadened by increasing the ratio of channel width towards unity at the cost of spatial efficiency for path-coiling as the width of the narrowest channel increases. In the limit of $\eta = 1$, the width of the channel remains unchanged and the transmission is always unity as it is shown in the figure, which corresponds to the case where the acoustic wave below the cut-off frequency travels in a lossless channel.

To experimentally validate our design approach, we fabricated labyrinthine cells with a conventional plastic 3D printer by extruding the 2D design in Figs. 1(b) and 1(c). We measured the performance of each acoustic unit cell by sending a sequence of Gaussian-modulated pulses at different center frequencies.[21] A detailed experimental setup can be found in the supplementary material. The transmitted pulses are detected both with and without the unit cell inside the tube at a sampling rate of 100 kHz, as shown in Figs. 5(a) and 5(c).

The detected signal is processed with MATLAB to retrieve properties of the unit cell. The transmission at a specific frequency is evaluated by Fourier transforming the time-gated signals and calculating the amplitude ratio in the frequency domain. The signal delay of the signal induced by the existence of the metamaterial unit cell is obtained by maximizing the correlation function of the two pulses. The

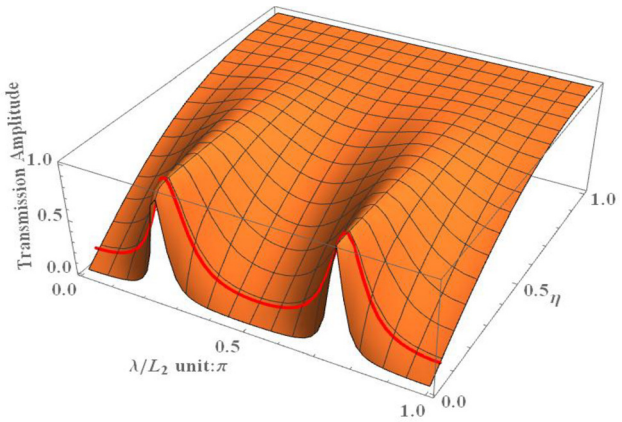

FIG. 4. The transmission envelope curve at different frequencies for the given channel width ratio η and the length of each IML. The red line corresponds to the envelope line for the cells we simulate and measure with $\eta = 0.062$.

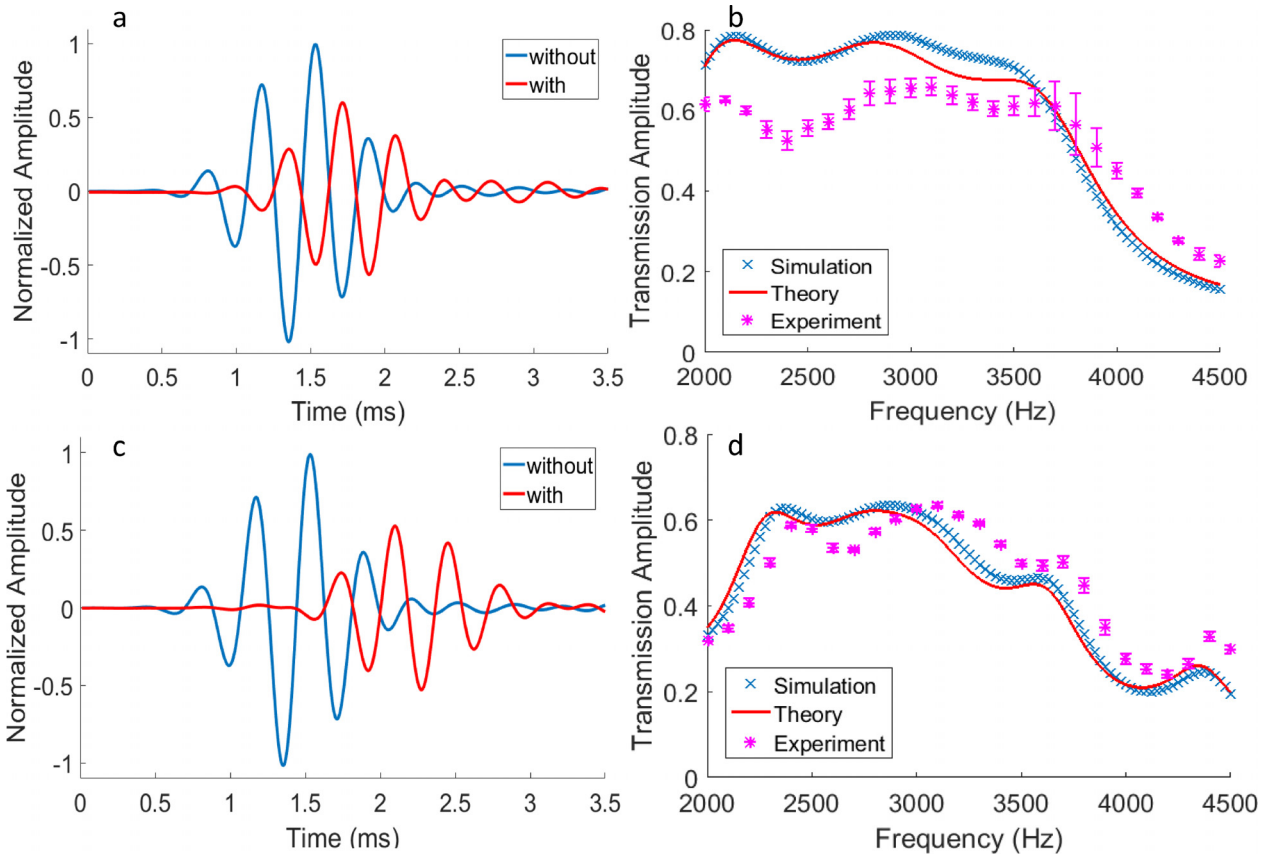

FIG. 5. Measured signal with and without the metamaterial unit cell and the retrieved transmission amplitude. (a) The emitted Gaussian-modulated pulse signal is detected with and without the unit cell design in Fig. 1(b) placed between the speaker and the detector. (b) The experimentally measured transmission is compared with the lossy result of simulation and theory. (c) Detected signals and (d) transmission for the unit cell design in Fig. 1(c).

effective refractive index is calculated by converting the signal delay to the effective path length. The comparison of simulation, theory, and experimental results is shown in Figs. 5(b) and 5(d). In the simulation, an empirical loss is added as the imaginary part of the wavenumber, i.e., $k_{lossy} = k_0 + 0.028\, ik_0$ to fit the experimental results, where k_0 is the original wavenumber. The complex wavenumber represents a transmitted amplitude of 0.839 after travelling over the effective path length of a wavelength inside the unit cell. The same imaginary part of the wavenumber is added in theory to derive the lossy transmission and the results show good consistency with the simulation in Figs. 5(b) and 5(d). The measurement is repeated 40 times and each time the signal is detected with four microphones. Although the peak transmission is not 100% due to unavoidable loss, the transmission amplitude preserves a flat line within a wide frequency band for both unit cells, validating the design approach for broadening the bandwidth. The measured refractive indices shown in Figs. 2(b) and 2(d) also remain roughly of the same value within the whole spectrum, ensuring a low dispersive property which is important in broadband wavefront engineering, such as acoustic lenses and holograms.[7,8,22]

IV. CONCLUSION AND DISCUSSION

In summary, we have developed a design approach for acoustic labyrinthine unit cells with an adjustable shared working frequency and bandwidth by introducing an internal impedance matching layer. The theory based on connecting tube structures is used to predict the lossless transmission and effective refractive index of the metamaterial unit cell. We simulate the acoustic labyrinthine cells using the Finite Element Method with COMSOL Multiphysics and the result shows good consistency with the theory. Both simulation and theory indicate that there exists an envelope line of the lowest transmission for labyrinthine unit cells with different narrowest channel lengths. The center frequency as well as the bandwidth of the envelope line can be tuned by adjusting the length of the IML as well as the inner and outer most channel width ratio. The theory presented here can serve as an efficient tool for metamaterial cell designs based on path-coiling. Two unit cells with a relatively low and high index are fabricated and measured and the experimental results confirm that the unit cells share a high transmission region over 1.4 kHz with low dispersive effective refractive indices. By modifying the number of layers or the shape of the IML, we can achieve a high transmission, broad bandwidth, and high index coverage design. It is hoped that the unit cells proposed here can find applications in various scenarios where high transmission and broadband functionality are desired.

SUPPLEMENTARY MATERIAL

See supplementary material for parameters of metamaterial unit cells simulated in Fig. 3(a) and details of the experimental setup for single unit cell measurement.

[1]Z. Liu, X. Zhang, Y. Mao, Y. Y. Zhu, Z. Yang, C. T. Chan, and P. Sheng, Science **289**(5485), 1734 (2000).
[2]S. A. Cummer, J. Christensen, and A. Alù, Nat. Rev. Mater. **1**(3), 16001 (2016).
[3]G. Ma and P. Sheng, Sci. Adv. **2**(2), e1501595 (2016).
[4]Y. Li, X. Jiang, R.-q. Li, B. Liang, X.-y. Zou, L.-l. Yin, and J.-c. Cheng, Phys. Rev. Appl. **2**(6), 64002 (2014).
[5]Y. Li, X. Jiang, B. Liang, J.-c. Cheng, and L. Zhang, Phys. Rev. Appl. **4**(2), 024003 (2015).
[6]Y. Tian, Q. Wei, Y. Cheng, and X. Liu, Appl. Phys. Lett. **110**(19), 191901 (2017).
[7]Y. Xie, C. Shen, W. Wang, J. Li, D. Suo, B.-I. Popa, Y. Jing, and S. A. Cummer, Sci. Rep. **6**(1), 35437 (2016).
[8]Y. Xie, W. Wang, H. Chen, A. Konneker, B.-I. Popa, and S. A. Cummer, Nat. Commun. **5**, 5553 (2014).
[9]Y. Li, S. Qi, and M. B. Assouar, "Theory of metascreen-based acoustic passive phased array," New Journal of Physics **18**(4), 043024 (2016).
[10]Y. Xie, A. Konneker, B.-I. Popa, and S. A. Cummer, Appl. Phys. Lett. **103**(20), 201906 (2013).
[11]X. Zhu, K. Li, P. Zhang, J. Zhu, J. Zhang, C. Tian, and S. Liu, Nat. Commun. **7**, 11731 (2016).
[12]Z. Liang and J. Li, Phys. Rev. Lett. **108**(11), 114301 (2012).
[13]Y. Li, B. Liang, X.-y. Zou, and J.-c. Cheng, Appl. Phys. Lett. **103**(6), 63509 (2013).
[14]P. Peng, B. Xiao, and Y. Wu, Phys. Lett. A **378**(45), 3389 (2014).
[15]W. Wang, Y. Xie, A. Konneker, B.-I. Popa, and S. A. Cummer, Appl. Phys. Lett. **105**(10), 101904 (2014).
[16]Y. Ding, E. Statharas, K. Yao, and M. Hong, "A broadband acoustic metamaterial with impedance matching layer of gradient index," Appl. Phys. Lett. **110**(24), 241903 (2017).
[17]K. Li, B. Liang, J. Yang, J. Yang, and J.-c. Cheng, Appl. Phys. Lett. **110**(20), 203504 (2017).
[18]L. E. Kinsler, A. R. Frey, A. B. Coppens, and J. V. Sanders, *Fundamentals of Acoustics*, 4th ed. (Wiley-VCH, 1999), p. 560, ISBN 0-471-84789-5.
[19]G. Du, Z. Zhu, and X. Gong, *Fundamentals of Acoustics* (Nanjing University Press, 2001).
[20]P. W. Jones and N. J. Kessissoglou, "A numerical and experimental study of the transmission loss of mufflers used in respiratory medical devices," Acoustics Australia **38**(1) (2010).
[21]B.-I. Popa, L. Zigoneanu, and S. A. Cummer, Phys. Rev. B **88**(2), 024303 (2013).
[22]C. Shen, Y. Xie, N. Sui, W. Wang, S. A. Cummer, and Y. Jing, Phys. Rev. Lett. **115**(25), 254301 (2015).